C.Bedon, G.Rinaldin, M.Izzi, M.Fragiacomo, C.Amadio (2015), "Assessment of the structural stability of Blockhaus timber log-walls under in-plane compression via full-scale buckling experiments". Construction & Building Materials, 78: 474-490.

Assessment of the structural stability of *Blockhaus* timber log-walls under in-plane compression via full-scale buckling experiments

C. Bedon[1], G. Rinaldin[2], M. Izzi[3], M. Fragiacomo[4], C. Amadio[5]

Abstract

Blockhaus structural systems are obtained by assembling multiple timber logs able to interact with each other by means of simple mechanisms (e.g. contacts, tongues and grooves, and carpentry joints, also referred to as 'corner' joints). Although these systems have ancient origins, the structural behaviour of *Blockhaus* systems under well-defined loading and boundary conditions is still complex to predict. The paper focuses on the assessment of the typical buckling behaviour and resistance of in-plane compressed timber log-walls. The effects of various mechanical and geometrical aspects such as in-plane rigid inter-storey floors, load eccentricities, different types of lateral restraints, openings (e.g. doors or windows) or additional metal stiffeners, are investigated by means of full-scale buckling experiments. Results are then critically discussed and preliminarily assessed via analytical formulations taken from classical theory of plate buckling and column buckling. Although further advanced studies are required for the development of a generalized buckling design method, it is shown that several mechanical and geometrical aspects should be properly taken into account to correctly predict the structural capacity of *Blockhaus* systems under in-plane compression.

Keywords: timber log-walls; full-scale buckling experiments; load eccentricity; carpentry joints; metal stiffeners; analytical models.

[1] Ph.D., Researcher. University of Trieste, Department of Engineering and Architecture, Piazzale Europa 1, 34127 Trieste, Italy. Corresponding author. Email: bedon@dicar.units.it.
[2] Ph.D., Research Fellow. University of Sassari, Department of Architecture, Design and Urban Planning, Piazza Duomo 6, 07041 Alghero (SS), Italy.
[3] Ph.D. Candidate. University of Trieste, Department of Engineering and Architecture, Piazzale Europa 1, 34127 Trieste, Italy.
[4] Associate Professor. University of Sassari, Department of Architecture, Design and Urban Planning, Piazza Duomo 6, 07041 Alghero (SS), Italy.
[5] Full Professor. University of Trieste, Department of Engineering and Architecture, Piazzale Europa 1, 34127 Trieste, Italy.

1. Introduction

Blockhaus (or log-haus, blockbau, etc.) structural systems represent a technology of ancient origins but used in modern practice for the construction of residential and commercial buildings, generally up to two levels (e.g. [1]). These structures are commonly obtained by assembling multiple timber logs stacked horizontally one upon each other, and the interaction between these basic components is provided by simple mechanisms such as tongues and grooves, carpentry connections, often referred to as 'corner' joints, friction phenomena and contact surfaces. Despite these basic mechanisms, from a practical point of view, currently available standards for the design of timber structures (e.g. [2]) do not provide analytical models for an appropriate verification of these structural systems. As a result, their effective behaviour and load carrying capacity under specific loading and boundary conditions is rather complex to properly predict. Due to the continuous research for aesthetically pleasing solutions in modern architecture, moreover, designers are often required to ensure specific architectural solutions which often contrast with pure structural requirements, hence demanding careful consideration and proper assumptions in calculations.

In the last years, few studies focused on *Blockhaus* structural systems. Experimental and numerical studies were dedicated, for example, to the assessment of the structural behaviour of log-walls under seismic loads [3][4]. These studies emphasized the high flexibility and damping capacity of the examined structural systems, as well as the importance of various mechanical and geometrical aspects on their global behaviour. Static friction experiments were discussed in [5], in order to assess the effectiveness of the possible dissipative mechanisms offered by timber logs in contact, when subjected to in-plane lateral actions such as seismic loads. Further preliminary studies [6][7] were also dedicated to the experimental investigation of log-walls under in-plane compressive vertical loads. Buckling may be a design issue as log-walls are typically characterised by high slenderness ratios compared to other structural systems, and low modulus of elasticity as timber is stressed in the perpendicular to the grain direction under gravity load. Buckling phenomena involve a complex interaction between strength and deformation capacities of structural members, and wide series of experimental studies and simplified analytical methods were proposed over the past years for the buckling behaviour of various timber structural systems (e.g. [9][10][11]). Buckling tests were performed also in [6, 7], on (1:4) and (1:1.4) scaled log-walls prototypes, in order to preliminarily assess the resistance

of *Blockhaus* structural systems under compression. Simple analytical formulations were also proposed, for an approximate calculation of the corresponding Euler's critical buckling load [7], with the recommended partial safety coefficient being calibrated on safety requirements of DIN standards for timber structures [8]. The experiments discussed in [6] and [7], however, were carried out on log-walls under mid-span concentrated loads, as well as on log-wall specimens laterally unrestrained at their top log (e.g. fully neglecting the restraint provided by inter-storey floors), hence typically resulting in significant underestimation of the actual buckling capacities.

In this work, based on earlier contributions [6][7], full-scale buckling experiments are performed on five different typologies of *Blockhaus* log-walls under in-plane compression. The five specimens differ for the number and position of door and window openings, as well as for the adopted lateral restraints, the presence of additional metal stiffeners, and the imposed load eccentricity. The major difference from buckling experiments discussed in [6][7], however, is given by the assumption of a more realistic distribution of loads (e.g. uniformly distributed compressive loads, rather than mid-span concentrated loads only) as well as of a restraint condition at the top of the examined log-walls typically associated to the presence of an in-plane rigid inter-storey floor. As highlighted in [12] and [13] by means of Finite-Element (FE) numerical studies validated on former experimental results [6][7], the presence of in-plane rather than fully flexible inter-storey floors typically provides increased flexural stiffness and, consequently, higher buckling resistance for the examined structural systems. As a result, the effects of this additional top support should be properly assessed and taken into account in calculations.

In this paper, the test results of the five full-scale walls tested under in-plane compression are presented and critically discussed. The test results are then assessed against analytical calculations performed by means of classical formulations derived from plate buckling and column buckling theoretical models [14][15]. The final aim of this on-going research project is the derivation of a generalized design buckling method of practical use for the verification of vertically loaded log-walls having different mechanical and geometrical properties (e.g. log cross-section, size and location of openings, load eccentricities), as well as restraint conditions (e.g. orthogonal log-walls, pillars, in-plane rigid diaphragms, etc.).

2. *Blockhaus* log-walls and structural systems

2.1. Geometrical and mechanical properties

In current practice, the typical *H*×*L Blockhaus* log-wall is obtained by assembling a series of spruce logs with strength class C24, according to [16] (e.g. Fig.1a). These logs, obtained by gluing together two 40mm-thick lamellas of spruce, are stacked horizontally one upon each other and have typical slender *b*×*h* cross-sections (with height *h* comprised between 160mm and 190mm, thickness *b* varying from 80mm and 240mm, and *h*/*b* ratios ≈ 1.6-2.4) characterized by small tongues and grooves. These tongues and grooves can have specific shapes, depending on the manufacturer, but their general aim consists in providing interlocking between the upper and lower logs in contact. A vapor-diffusible adhesive able to satisfy requirements of standards [17] is also used to ensure an appropriate structural interaction between the glued lamellas.

Each main log-wall is usually attached to a concrete foundation slab by means of steel angle bracket connectors offering an appropriate resistance against in-plane shear loads (e.g. one angle bracket every ≈1.5m width of wall [4]). The typical angle bracket used in practice by [1], for example, is 3mm thick, and is joined to the bottom timber log of the main wall and to foundation by means of twelve 4mm diameter, 60mm long nails and two M10 metal bolts, respectively. The structural interaction between the so assembled main log-walls and the orthogonal log-walls is then ensured by corner joints (e.g. [4]). Several joint solutions derived from tradition – able to respond to both structural and aesthetic requirements – are often realized in modern *Blockhaus* structures. Independently of their geometrical configuration, however, the general aim of these corner joints consists in providing a full interaction between the intercepting logs, so that all the timber components could behave as a fully coupled structural system, despite the absence of metal connectors among the logs. In *Blockhaus* buildings, moreover, permanent gravity loads are transferred onto each main log-wall to the foundation by inter-storey floors which typically realize an in-plane rigid diaphragm (e.g. by using OSB panels and timber joists, or glulam panels arranged on their edges) able to restrain the out-of plane deflections of the top logs (Fig.1b).

2.2. Susceptibility of *Blockhaus* log-walls to buckling phenomena

Compared to other structural systems and walls composed of traditional construction materials (e.g. masonry or concrete), the structural response of timber log-haus walls under in-plane compression and their susceptibility to buckling phenomena has been the subject of little research over the past years [6, 7]. Furthermore, no information on the design of log-walls is provided in current design standards of timber structures (e.g. [2]). The very low modulus of elasticity (MOE) of timber in the direction perpendicular to grain $E_{\perp}$ [16] (≈ 1/100 the compressive MOE of masonry or concrete), together with the usually high H/b ratio of *Blockhaus* log-walls, could lead to premature collapse mechanisms. The limited compressive resistance in the direction perpendicular to grain could also result in local crushing and damage. Careful consideration should then be given to the effects of possible load eccentricities. Although the typical intersection between the main log-walls and the floor joists provides a full interaction between them (Fig.1b), sometimes – due to architectural requirements – the same joists are interrupted within the log-wall thickness (Fig.1c).

Since metallic connectors are generally avoided or minimized in *Blockhaus* structural systems, it is clear that the typical log-wall can sustain the vertical loads as far as a minimum level of contact and interaction among the overlapping logs is guaranteed. At the same time, it is expected that the flexural behaviour of in-plane compressed log-walls would manifest limited flexibility and resistance, compared to '*fully monolithic*' timber walls. Finally, further issues could be represented by openings of doors and windows, since involving an interruption of timber logs and further discontinuity among the load carrying components of the investigated structural systems.

3. Full-scale buckling experiments

3.1. Specimens

In this work, five full-scale *Blockhaus* specimens were tested. Specimens having the same overall dimensions L= 4m × H= 2.945m and thickness b= 0.08m ('Tirol' logs, Fig.1a), but differing in terms of (i) lateral restraints; (ii) presence of additional metal stiffeners and (iii) presence of door and window openings, were compared (Table 1).

The 'reference' *Blockhaus* specimen W01, specifically, consisted of 16 main logs laterally restrained by two orthogonal log-walls (Fig.2). In order to avoid possible uplift and detachment or overturning of the upper logs during the experiments, the two top logs were fixed to each other by means of inner screws, equally spaced along the log-wall width *L* (Fig. 2a). This solution generally represents one of the few introductions of metal components in *Blockhaus* buildings (e.g. at the level of inter-storey floors and roofs [1]).

The structural capacities of the log-wall W01 under in-plane compressive loads were then compared to the buckling behaviour of an identical log-wall strengthened by means of three additional S235 grade steel, rounded dovetail profiles (specimen W02, Figs.2a and 3, Table 1), filled with spruce dovetails and introduced were the maximum out-of-plane deflections are expected (e.g. *L*/2, Fig.3a).

While the wood infills avoid possible yielding of the metal stiffeners, in current practice [1] the same steel dovetails are not rigidly connected to the adjacent logs, hence the structural interaction between them is provided by contacts and friction phenomena only.

In the case of specimens W03 and W04, door and window openings were introduced and differently positioned along the nominal width *L* of the reference sample W01 (Fig.2a and Table 1). The main characteristic of log-walls with openings [1] is given by steel hollow profiles introduced along the vertical edges of door and window openings(Figs. 2a and 4), so that a certain level of flexural stiffness for the entire log-wall, as well as a partial interaction among the interrupted logs, could be preserved. As for the case of sample W02, however, to ensure possible adjustment or expansions of timber components due to shrinkage or creep phenomena, these stiffeners are not rigidly connected to the adjacent logs and their structural effectiveness fully depends on contact mechanisms only.

Specimen W05, finally, was characterized by the presence of two continuous pillars composed of C24 spruce and obtained by gluing together four lamellas (Figs.5a and 5b). The base of pillars is usually suspended from the floor (Fig.5c), to ensure possible vertical adjustment (settlement) of the main log-wall during the building life-time due to shrinkage and creep deformations. In order to provide maximum bending stiffening contributions to the main log-wall, moreover, the grain of the pillars is vertically oriented and the pillar-to-wall interaction is guaranteed by C24 spruce rounded dovetails (Fig-5b).

3.2. Test setup and loading protocol

The full-scale experiments were performed at the Laboratory of Structural Engineering of the University of Trieste (Italy), Department of Engineering and Architecture, during June and July 2014, in non-controlled environment. The typical duration of buckling experiments was in the range 8-10 minutes and an appropriate setup was developed, to provide the desired loading and boundary conditions to the tested log-walls.

Blockhaus log-walls were positioned on the strong floor (Fig.6a) and the in-plane compressive load N – continuously monitored by means of a load cell – was applied by means of five hydraulic jacks properly distributed along the width L.. At the interface between the timber top logs and the hydraulic jacks, five steel plates (20mm thick) were introduced to prevent possible crushing mechanisms in the top timber log. Further timber supports were also rigidly connected to the upper log of each specimen (e.g. where the hydraulic jacks were positioned), so that the desired load eccentricities ($e_{load} \approx b/2 = 40$mm for all the specimens, with the exception of $e_{load} \approx b/5 = 15$mm for the log-wall W03) could be applied. After a first loading-unloading cycle up to ≈30kN, the compressive load N was increased – with almost a constant speed – up to failure.

During the experiments, to provide to the tested log-walls a top restraint condition comparable to an in-plane rigid inter-storey floor, two metal bracing systems were also introduced at ≈1/3 the log-wall width L (Figs.6a and 6b), so that the lateral displacement of top log could be prevented by 4 ϕ16 threaded bars. In this manner, each tested log-walls was able to freely deform in the direction of the applied compressive loads N, while possible out-of-plane deflections of the top log – due to high axial stiffness of the used threaded bars – were avoided. Test measurements (e.g. horizontal displacements at the mid-span section of the laterally restrained top logs, control point P04 (Fig.6a)) typically resulted in very small and almost negligible out-of-plane deformations, compared to the overall deformed shape of the main log-walls, hence confirming the validity of the adopted setup. Out-of-plane and in-plane deformations were in fact properly monitored during each buckling test and 14 linear voltage displacement transducers with a resolution of 0.01mm were used (Fig. 6a).

4. Full-scale test results

The behaviour of the tested log-walls generally showed large dependency on the specific geometrical configurations and on the applied load eccentricities.

4.1. Specimen W01

Specimen W01 failed at the attainment of a maximum compressive load N_{max}= 233.2kN (Fig.7).

Up to failure, the log-wall showed the typical 'plate buckling' deformed shape of a fully monolithic, in-plane compressed plate simply supported at the top and bottom edges, and almost clamped along the lateral vertical edges, due to the adopted 'Standard' corner joints. As a result – although affected by the introduced load eccentricity e_{load}– the obtained deformed shape was mainly characterized by maximum out-of-plane displacements attained near the centre of the log-wall (control point P06, Fig.7).

Collapse of the log-wall occurred due to partial cracking and progressive detachment of the three top logs (Fig.8), although the specimen manifested appreciable flexibility ($u(N_{max})/H \approx$ 0.016) and no damage occurred in the 'Standard' corner joints nor in the tongues and grooves of logs. Due to the flexural deformed shape attained in the main log-wall at failure, minor damages were found only at the external ends of the 4 top main logs (Fig.8b), as well as a beginning of crushing (Fig.8c) and a partial overturning (Fig.8b) were noticed, at the end of the experiment, in few top orthogonal logs.

4.2. Specimen W02

Up to failure, the deformed shape obtained for the log-wall W02 resulted almost comparable to that of specimen W01. An appreciable structural effectiveness of the adopted metal stiffeners, however, was noticed. The sample attained a maximum compressive load N_{max}= 240.1kN (Fig.9), and successively failed at N_u= 232.5kN due to progressive flexural damage of its upper top log (Fig.10).

This failure mechanism of the top timber log resulted mainly located near the lateral ends of the tested log-wall, where the out-of-plane deformations were prevented by the orthogonal log-walls through the adopted 'Standard' corner joints (Fig.10a). The same damage mechanisms propagated also towards the external portion of the top log, at both the log-wall ends (Fig.10b). Concerning the three steel rounded dovetail

stiffeners, no sign of damage or residual deformations were noticed in two of them (e.g. the bottom and the middle profile). Conversely, the upper stiffener manifested a partial yielding mechanism (Fig.10c) and a marked overall flexural deformation, having to prevent the maximum out-of-plane deflection of the tested log-wall. The hardwood timber dovetails introduced in each metal profile provided an appreciable contribution in fully avoiding possible compressive damages in the three metal profiles, hence ensuring their structural effectiveness up to failure.

4.3. Specimen W03

Specimen W03 typically manifested the collapse buckling mechanisms of a column (e.g. the portion of log-wall comprised between the openings) under eccentric compression. As shown in Fig.11, the maximum out-of-plane deflections were attained at the control point P06 (e.g. mid-span section of the central column). Although subjected to a low load eccentricity, compared to specimens W01 and W02, the log-wall W03 highlighted higher buckling resistance (N_{max}= 228.7kN) and marked flexibility up to failure ($u(N_{max})$≈ 0.032), due to the important stiffening contribution of the steel hollow profiles.

Collapse occurred due to progressive damage in tension perpendicular to grain in the main timber log located at the bottom edge of the window (Fig.12a). The almost local failure mechanism of this single timber log resulted then in the abrupt collapse of all the upper beams (final configuration of Fig.12a). Despite the observed collapse mechanism, the specimen W03 manifested an appreciable flexural interaction between logs and the central steel profiles (e.g. Fig.12b), and a fairly stable behaviour up to failure. During the experiment, the lateral portions of the main log-wall and the external metal profiles remained almost undeformed, hence suggesting the prevalent load-bearing role of the 'composite column' comprised between the openings.

4.4. Specimen W04

Exemplificative test results obtained for the specimen W04, differing from the log-wall W03 for the distance between the openings and for the amplitude of the assigned load eccentricity, are displayed in Fig.13.

Although the sample W04 globally attained a maximum compressive load N_{max} very close to the buckling resistance of specimen W03, this experiment highlighted a critical local mechanism at the connection between the central portion of the main log-wall and its overlapping top logs (Fig.14), which should be properly taken into account in the design of *Blockhaus* structural systems. This effect, probably due to the extremely reduced portion of logs in contact at the top edge of door and window openings (e.g. contact surfaces of nominal dimensions L_i=0.3m × b=0.08m), resulted in marked out-of-plane flexural deformations of the three 'Tirol' top logs, as well as in the contemporary partial overturning of the central column of the wall, thus in the progressive detachment between these portions (Fig.14b). The further partial, disjointed involvement of the portions of the wall near the lateral restraints contributed to sustain appreciable maximum compressive loads (N_{max}= 211.9kN), but typically resulted in an overall unstable deformed configuration of the specimen.

4.5. Specimen W05

Specimen W05 was finally tested in order to assess the structural effectiveness of timber pillars replacing the orthogonal log-walls and the traditional 'Standard' corner joints. The log-wall highlighted high buckling resistance (N_{max}= 221.3kN, Fig.15), almost comparable to that of the reference specimen W01.

Due to the adopted lateral restraints, conversely, collapse of the log-wall resulted in an almost brittle mechanism markedly different from samples W01 and W02.

In terms of overall flexural behaviour, due to lack of orthogonal log-walls able to provide a sort of an almost continuous clamp support, specimen W05 globally resulted comparable to an 'assembled', laterally stiffened column under compression, rather than a laterally restrained plate. This effect can be seen also from Fig.16, for example, where the out-of-plane displacements along the horizontal cross-section P02-P06-P09 are compared, at failure (e.g. N/N_{max}= 1), for specimens W01 and W05.

As shown, 'Standard' joints provides a more efficient lateral restraint to timber logs, hence resulting in maximum out-of-plane deflections at the centre of the log-wall W01 (e.g. P06 in Fig.16). Conversely, timber pillars appeared less efficient than orthogonal log-walls and 'Standard' joints, thus resulting in more uniformly distributed out-of-plane deformations among the log-wall surface (e.g. comparable maximum

displacements, for specimen W05, attained at the control points P02 and P06). From the same Fig.16, a partial unsymmetrical collapse mechanism for the log-wall W05 can also be noticed (e.g. P02 and P09 displacement amplitudes). Careful analysis of test measurements and acquired images (Fig.17) confirmed in fact the occurring of crack initiation along the left timber pillar (e.g. the side of log-wall where the P02 control point was located).

Collapse, specifically, occurred due to the progressive failure of timber rounded dovetails (starting from the top of the wall, towards the base) which are used in practice to provide the structural interaction between pillars and main 'Tirol' logs. An almost abrupt and brittle collapse mechanism characterized the experiment (Fig.17), and a large number of rounded dovetails failed due to tensile stresses in the direction perpendicular to grain. Damage mainly occurred where the cross section of dovetails has minimum size and the two trapezoidal lamellas are glued together (Fig.18).

4.6. Comparative discussion of full-scale test results

Full-scale buckling experiments globally demonstrated an appreciable resistance and buckling behaviour of the examined log-walls, although highlighting some critical mechanisms in few of them. Results are compared in Table 2 for each specimen in terms of maximum compressive load N_{max} and corresponding out-of-plane deformation $u(N_{max})$. The flexibility, effectiveness of lateral end restraints and metal stiffeners, as well as the susceptibility of each specimen to the assigned load eccentricities e_{load}, are also provided in Table 2 in the form of initial flexural stiffness K derived from full-scale test measurements.

Further comparisons are then proposed in Fig.19 in terms of maximum envelope of out-of-plane deformations u-to log-wall height H ratio, plotted against the applied compression load N, while related comments are given in Sections 4.6.1 and 4.6.2.

4.6.1. Effect of lateral restraints and additional metal stiffeners

Compared to log-walls without openings, the reference specimen W01 demonstrated an initial flexural stiffness K almost intermediate between W02 (metal dovetails) and W05 (timber pillars) specimens, as highlighted in Table 2 and Figure 19a.

Timber pillars provided in fact an appreciable stiffening contribution to the tested log-wall W05 – especially in the first loading phase – almost comparable to orthogonal log-walls with 'Standard' corner joints. However, the same specimen showed a critical, brittle failure mechanism in timber rounded dovetails which resulted in an abrupt global collapse and null residual strength of the wall (Fig.19a). This phenomenon should be properly taken into account, since the progressive failure of rounded dovetails (not directly visible, due to the presence of pillars) resulted in an almost unexpected collapse of the entire log-wall.

Conversely, the introduction of steel metal dovetails (W02) provided a ≈40% increase in initial stiffness K and a moderate increase (≈3%) of maximum load carrying capacity (N_{max}), compared to the unreinforced W01 specimen (Table 2 and Fig.19a). Although further studies are required for a proper optimization of possible additional metal stiffeners, it is clear that their introduction could provide improved structural capacities to the examined structural systems.

In terms of overall deformed shapes obtained for the same log-walls, detailed analysis of test measurements confirmed the occurrence of a sort of plate buckling mechanism (Figs. 20a and 20b). Fig.20a, in particular, shows the out-of-plane deformations monitored along the mid-span vertical axis of log-wall W01 (control points P04-P07) – as a ratio of the wall height H – versus the distance z of the control point from ground. Different curves are associated to specific loading ratios N/N_{max}. Fig.20b, conversely, displays the maximum deformed shape at failure (N/N_{max}= 1) for specimens W01, W02 and W05. As shown, the out-of-plane displacements at point P04 are almost null, or negligible, up to failure of specimens, demonstrating the effectiveness of the adopted lateral restraint and metal bracings (Section 3). At the same time, maximum out-of-plane deformations are obtained at control points P05 and P06, as a direct consequence of the applied load eccentricity e_{load}.

4.6.2. Effect of door and window openings

Buckling experiments also emphasized that door and window openings can markedly modify the global behaviour of *Blockhaus* log-walls (Fig.19b). Compared to the log-wall W01, for example, specimen W04 manifested a ≈30% decrease in initial stiffness K, due to the minimized distance L_i between the openings,

and a≈10% decrease in buckling resistance N_{max}, due to the beneficial contribution of the hollow steel profiles, although a local failure mechanism rather than a global collapse was noticed.

The assigned load eccentricities e_{load} affected the structural response of all the specimens, throughout the experimental programme. Consequently, test results obtained for the log-wall W03 (e_{load}= 15mm) are not directly comparable to the other samples (e_{load}= 40mm). For the same reason, as proposed in Table 2 and Fig.19b, the initial stiffness K of log-wall W03 is approximately twice that of specimen W01 without openings, and the corresponding buckling ultimate resistances N_{max} are almost comparable (≈2% of difference). However, specimen W03 showed a markedly different buckling behaviour compared to the other samples. As shown in Fig.21, in fact, maximum deflections are located at the centre of the log-wall (P06) and the overall out-of-plane deformed shape measured at points P04-P07 typically recalls the flexural behaviour of a column loaded in compression (Fig.21a). The lateral portions of the log-wall and also the orthogonal log-walls, conversely, are hardly involved in the global failure mechanism of specimen W03, giving the lower out-of-plane deformations (e.g. P03 in Fig.21b).

5. Mechanical characterization of timber

Further experiments [18] were performed on small specimens of *Blockhaus* components, in order to properly characterize the base material used in the tested *Blockhaus* timber log-walls, being the elastic properties of spruce of primary importance for further analytical and numerical validation of the full-scale predictions. More specifically, the main elastic moduli $E_{\perp}$ and $E_{||}$, as well as ultimate compressive resistances $\sigma_{u,\perp}$ and $\sigma_{u,||}$ of timber components, in the direction perpendicular and parallel to grain respectively, were measured by means of uniaxial compressive tests (Section 5.1), while the longitudinal shear modulus G of spruce was derived from bending experiments (Section 5.2), being all these parameters directly involved in the flexural deflection of the studied log-walls.

5.1. Compressive tests

A total number of 12 specimens were taken, respectively, from (a) main 'Tirol' logs (6 specimens), (b) pillars (3 specimens) and (c) rounded dovetails (3 specimens). 'Tirol' log specimens were directly obtained

from the log-wall beams, thus the typical sample resulted in a 80mm × 180mm cross-section (e.g. nominal profile of Fig.1a deprived of small tongues and grooves along the top and bottom surfaces), being l_{log}= 120mm the nominal length. Pillar specimens, similarly, were obtained from their current cross-section deprived of the rounded dovetail notch (Fig.5b), so that each sample resulted in a 80mm × 160mm base section, with h_{pillar}= 180mm being its nominal height. Small samples of rounded dovetails, finally, were obtained by reducing their nominal height (Fig.5b) to a reference size $h_{dovetail}$= 180mm.

Monotonic, quasi-static compressive loads *N* were applied to all the samples, and linearly increased up to failure. During the tests, the corresponding shortening of specimens was continuously measured on two opposite faces. Based on the loading configuration of timber logs in full-scale *Blockhaus* specimens subjected to in-plane compressive loads, the mean MOE perpendicular to grain $E_{\perp}$ and the ultimate compressive strength of timber in the same direction $\sigma_{u,\perp}$ were estimated for type (a) specimens [18]. In the case of specimens (b) and (c), on the contrary, samples were subjected to compressive loads *N* acting in the direction parallel to grain. The mean MOE $E_{\parallel}$ and failure stress $\sigma_{u,\parallel}$ were then calculated as for samples (a). Test results are listed in Tables 3 and 4 respectively.

Specimens generally showed an almost stable behaviour up to failure (Figs.22a-22b). In the case of pillar (b) and dovetail (c) specimens (Table 4), the tested samples showed an average MOE $E_{\parallel,\text{mean}}$ in good agreement with the corresponding nominal value provided in standard recommendations for structural timber components [16]. The same specimens also manifested an ultimate failure strength in the direction parallel to grain equal to 32.8N/mm^2 and 50.1N/mm^2 respectively, thus markedly larger than the characteristic value suggested by standards for C24 spruce ($f_{c,0,k}$= 24 N/mm^2 [16]). Test measurements on 'Tirol' log specimens, otherwise, resulted in a mean MOE $E_{\perp}$ markedly lower than expected ($E_{90,mean}$= 370 N/mm^2 [16], Table 3). In terms of ultimate stress, the same specimens failed at $\sigma_{u,\perp}\approx$ 3.4N/mm^2 and the typical collapse mechanism is showed in Fig.22b. These series of experiments, in particular, highlighted high sensitivity of the measured mechanical properties to the shape of 'Tirol' cross-sections. Failure typically occurred at the interface between the glued lamellas (e.g. Fig.22a) and the corresponding MOE values (Tables 3-4) showed marked variability from their average value. In order to estimate the longitudinal shear modulus *G*, consequently,

further experiments were carried out separately (Section 5.2), and preferred to a rough calculation derived from compressive tests only (e.g. $G \approx E_{||} / 16 = 722$MPa [20], with $E_{||}$ given in Table 4).

5.2. Bending tests

The average shear modulus G, specifically, was calculated by means of four-point bending experiments carried out on additional 14 small specimens of 'Tirol' logs (Fig.22c), by using the 'variable span method' [18], that is estimating:

$$G = \frac{1.2}{K_1} \tag{1}$$

with

$$K_1 = \frac{1}{E_{app}} \Big/ \left(\frac{h}{L}\right)^2 \tag{2}$$

$$E_{app} = \frac{L^3 \Delta F}{48 I \Delta w}, \tag{3}$$

where h, L are the section depth and span of specimens; I their second moment of area and ΔF, Δw the measured loads and mid-span deflections in the elastic phase of experiments (Fig.22c). An average shear modulus G= 617MPa, markedly lower than $G \approx E_{||} / 16 = 722$MPa [20], was obtained and taken into account for further calculations.

6. Comparison of full-scale test results against analytical formulations

Assessment of full-scale experiments was successively carried-out using simplified formulations derived from classical theory. In order to take into account the structural effect of the additional top restraint representative of in-plane rigid inter-storey floors, equations were derived from plate buckling and column buckling classical formulations [14][15].

6.1. Log-walls without openings

For timber log-walls without openings, simplified calculations were performed by means of classical theory of isotropic thin plates, continuously restrained along the four edges and subjected to in-plane uniformly distributed pressures of equivalent load *N*.

This approach allows in fact for the implementation of the top restraint provided by in-plane rigid floors. Conversely, it does not allow a proper estimation of interlocking effect between multiple logs, since each log-wall is regarded as a '*fully monolithic*' isotropic wall having thickness *b*, height *H*, width *L* and critical buckling load given by [14]:

$$N_{cr} = N_{cr,0}^{(E)} \cdot \chi_{imp} = \left(k_{\sigma} \frac{\pi^2}{12} \frac{b^3}{L} \frac{E_{\perp}}{\left(1 - \left(\frac{E_{\perp}}{2G} - 1\right)^2\right)} \right) \cdot \chi_{imp} \quad (4)$$

being $E_{\perp}$ the average MOE perpendicular to grain and *G* the average shear modulus, and [13]:

$$\chi_{imp} = \left(1 - \frac{e}{b}\right), \quad (5)$$

with $e = e_{load}$ a parameter calibrated to take into account the effects of initial curvatures or load eccentricities.

In Eq.(4), moreover, k_{σ} is a buckling coefficient describing the effects of various lateral end restraints, and should be properly calculated. Based on the effective restraint provided by orthogonal log-walls and 'Standard' joints, as well as on the earlier FE assessment provided in [13], k_s could be assumed equal to 6.97, like for a plate simply supported at the top-bottom edges and clamped along the vertical edges.

Although the χ_{imp} imperfection factor of Eq.(4) was proposed in [13] to describe the effects of possible geometrical curvatures or load eccentricities, the critical load N_{cr} provides poor information on the actual load carrying capacities of the studied log-walls. At the same time, the structural effectiveness of additional metal rounded dovetails (e.g. specimen W02), as well as their interaction with the adjacent timber logs in contact, cannot be explicitly taken into account. Finally, possible effects due to timber anisotropy – roughly described in Eq.(4) in the form of an equivalent isotropic, indefinitely linear elastic material – are not properly described. As a result, FE static incremental analyses, inclusive of friction phenomena and full

mechanical characterization of timber, would be necessary to appropriately investigate the structural behaviour of the examined log-walls up to failure.

In this context, further simple and approximate calculations could be again derived from the theory of in-plane compressed thin plates. Based on Wolmir theoretical model [15], for example, the compressive load N – maximum lateral displacement u_{max} of a monolithic $L \times H \times b$ plate subjected to initial geometrical imperfections of maximum amplitude u_0 and continuously supported along the four edges is given by:

$$N = E_{\perp} L \left(\frac{b}{H}\right)^2 \left\{ \frac{\pi^2}{3\left(1-\left(\frac{E_{\perp}}{2G}-1\right)^2\right)} + \frac{\pi^2}{8}\left[\left(\frac{u_{\max}}{b}\right)^2 + 3\left(\frac{u_{\max}}{b}\frac{u_0}{b}\right) + 2\left(\frac{u_0}{b}\right)^2\right] \right\} \frac{u_{\max}}{u_{\max}+u_0}. \qquad (6)$$

The main advantage of Eq.(6) is that initial imperfections are properly taken into account, although the same equation applies to isotropic, "*fully monolithic*" plates only, with simply supports along all the edges.

Comparative experimental and analytical plots are proposed in Fig.23, where deformations measured at control point P06 for the specimen W01 are compared to analytical calculations obtained from Eqs.(4) and (6) in the form of critical load N_{cr} and load N-maximum displacement u_{max} (with $u_0 = e_{load}$) respectively.

In both Eqs.(4) and (6), the average MOE $E_{\perp}$ and shear modulus G derived from experiments on small specimens were taken into account (Sections 5.1 and 5.2).

As shown, initial imperfections and boundary conditions can markedly affect the global behaviour of the examined log-walls. The predicted critical load $N_{cr,}$ (Eq.(4)) provides in fact close agreement with test predictions once the assigned eccentricity is properly described by means of Eq.(5). At the same time, Eq.(4) emphasizes the fundamental role of the additional top lateral restraint provided by in-plane rigid inter-storey floors. Analytical predictions based on Heimeshoff and Kneidl theoretical approach [7] – fully neglecting the important role of this latter top support – would in fact largely underestimate the actual load carrying capacity of specimen W01 (Fig.23 and Table 5). As shown in Table 5, conversely, calculation of the pure compressive resistance N_c of the same log-wall – as the compressive resisting surface multiplied by the average experimental resistance $\sigma_{u,\perp}$ (Table 3) – would not properly capture the susceptibility of all the investigated specimens to buckling failure mechanisms.

In terms of load-displacement response (Eq.(6)) of the same log-wall W01, Fig.23 further highlights the importance of a proper description of geometrical imperfections and load eccentricities, as well as an appropriate mechanical calibration of timber elastic properties, thus resulting in an accurate estimation of the initial elastic stiffness *K*. Conversely, the same analytical method does not take into account possible effects deriving from timber progressive damage or detachment of the logs in contact, and consequently the curves displayed in Fig.23 only roughly describe the structural behaviour of specimen W01 up to failure.

6.2. Log-walls with double openings

In the case of in-plane compressed *Blockhaus* log-walls with double (e.g. door and window) openings, simple analytical estimations for the assessment of their load carrying capacities were derived from classical theory of column buckling [14]. Full-scale experiments discussed in Section 4 highlighted in fact that the portion of log-wall comprised between the openings has a prevalent role in the load-carrying behaviour of the entire specimen and can be considered as a 'composite' column, where the equivalent flexural stiffness EI_{ef} depends on both the timber and flexural contributions of the steel profile:

$$EI_{ef} = E_{\perp} \frac{b^3 L_i}{12} + 2E_{steel} I_{steel}, \tag{7}$$

being $E_{\perp}$ and E_{steel} the MOE of timber in the direction perpendicular to grain and steel respectively, with I_{steel} the second moment of area of a single metal stiffener (Fig.4).

As a result, the critical load N_{cr} and the out-of-plane deflections *u(z)* at a given control point (with $0 \le z \le \overline{H}$) – due to the applied compressive load *N*– could be respectively estimated as [13]:

$$N_{cr} = N_{cr,0}^{(E)} \cdot \chi_{imp} = \left(\frac{\pi^2 \left(EI_{ef} \right)}{\overline{H}^2} \right) \cdot \chi_{imp} \tag{8}$$

with χ_{imp} given by Eq.(5), and

$$u(z) = u_0 \sin\left(\frac{\pi z}{\overline{H}} \right) \frac{N \overline{H}^2}{EI_{ef} - N \overline{H}^2}, \tag{9}$$

where u_0 denotes in Eq.(9) the maximum amplitude of geometrical imperfections or eccentricities (u_0= 1.25 × e_{load} [14]).

In Eqs.(8) and (9), finally

$$\overline{H} = \beta \times H_{ref} \tag{10}$$

signifies the effective buckling length for the 'equivalent column' and should be properly calculated based on its reference height H_{ref}, on the height H_d and H_w of door and window openings, as well as on the effective end supports of the examined portion of log-wall (e.g. β coefficient [14]).

Calculations derived from Eqs.(8) and (9) are proposed in Table 5 and Fig.24.

In Fig.24, specifically, test results obtained for specimens W03 and W04 are compared to analytical calculations obtained from Eq.(9), in the form of u /H ratio versus the applied load N, assuming for timber and steel the mean experimental ($E_{\perp}$ given by Table 3) and nominal (E_{steel}= 210GPa) MOEs respectively.

The difference among the three analytical curves of Fig.24 is given by the boundary condition and reference height H_{ref} taken into account by means of Eq.(10). Plot (I) refers to a $H_{ref} \equiv H_w$ high column, clamped at the base and simply supported at the top end (β= 0.699 in Eq.(10) [14]). Plot (II), conversely, is obtained by taking into account the same clamp-pin condition (β= 0.699 in Eq.(6) [14]), but the reference height $H_{ref} \equiv H_w$ of the window only. Plot (III), finally, assumes for the reference column an equivalent height $H_{ref} \equiv H_d$ (door size), and the condition of clamped-supported ends (β= 1 in Eq.(10) [14]). This assumption, specifically, totally neglects the possible restraint contribution offered by the interrupted timber logs above the window.

As shown in Fig.24, the proposed analytical approach only roughly describes the global behaviour of the tested log-walls, particularly for the specimen W04, which failed due to a local mechanism. For the specimen W03, which collapsed due to a global buckling mechanisms, it can be seen otherwise that the overall response of the log-wall is governed by the H_w high column (plots (I) and (II) of Fig.24a), but its actual restraint condition is intermediate between a clamp-pin (I) and a simply supported (II) condition.

For the same specimens W03 and W04, further analytical calculations are proposed in Table 5. In it, the analytical model presented in [7], since not able to take into account the strengthening contribution due to the inter-storey floors, as well as the flexural contribution of the steel hollow profiles, typically results in a marked overestimation of the actual resistances obtained from experiments (Table 5, (ii)). Eq.(8), although accounting for the assigned load eccentricity (Eq.(5)), provides an approximate prediction of the expected buckling failure load (Table 5, (I) and (II)). Fully neglecting the restraint contribution of the timber logs

above the window (Table 5, (III)), otherwise, would not properly describe the observed buckling behaviour, as well as strongly underestimate the corresponding buckling resistance. The rough calculation of the pure compressive resistance N_c only for the same specimens (Table 5, (iii)), finally, would result in a marked overestimation of the actual load carrying capacities for the studied log-walls, hence confirming the importance of a proper assessment of their buckling behaviour and resistance.

7. Conclusions

In the paper, full-scale buckling experiments performed on five different timber *Blockhaus* log-walls under eccentric in-plane compressive loads were presented and critically discussed. The main difference between the tested log-walls was given by the overall geometry of the specimens (e.g. presence and position of door and window openings), the adopted lateral corner joints and restraints (e.g. orthogonal log-walls or timber pillars), the imposed load eccentricities and the presence of additional metal stiffeners. As shown, all these parameters can affect the global buckling behaviour of the examined structural system. In any case, the tested samples generally manifested high buckling resistance and – in most cases – large flexibility up to failure. The tested walls, in particular, although composed of multiple logs interacting together by means of contacts and friction mechanisms only, manifested an appreciable stable behaviour up to the occurrence of the first failure mechanisms. Conversely, differing from "*fully monolithic*" timber walls, all the full-scale experiments resulted in collapse configurations strictly related to the examined structural system (e.g. unconnected timber logs stacked horizontally). Comparative analytical and experimental calculations were also proposed, based on analytical methods derived from classical theory of plate and column buckling and on the average mechanical properties of timber obtained from additional small specimens.

As shown, existing analytical models for "*fully monolithic*" panels and columns can provide only approximate estimation of the expected load-carrying behaviour of *Blockhaus* log-walls under in-plane vertical loads. Several mechanical and geometrical aspects, namely related to timber anisotropy, interaction between logs, effective boundary restraint provided by the adopted corner joints or initial geometrical imperfections and load eccentricities, should in fact be properly taken into account. A rough calculation of the pure compressive resistance of the same log-walls, conversely, would not properly capture their

susceptibility to buckling failure mechanisms, hence resulting in a marked and non-conservative overestimation of their actual load carrying capacities. Although further extended studies are required to fully understand the effects of several variables on the load carrying behaviour of log-walls under compression, it is expected that critical and extended discussion of full-scale experiments and analytical calculations could represent a valid background for future investigations aimed to develop simplified design buckling methods for in-plane compressed log-walls.

Acknowledgements

Rubner Haus AG SpA is gratefully acknowledged for financial support. Dr. Annalisa Battisti (Rubner Haus), Dr. Franco Trevisan (University of Trieste) and Dr. Andrea Cernigoi (University of Trieste) are also gratefully acknowledged for the technical support during planning and execution of experiments performed at University of Trieste, Department of Engineering and Architecture (DICAR) on full-scale and small *Blockhaus* specimens.

References

[1] Rubner Haus AG SpA. www.haus.rubner.com

[2] EN 1995-1-1:2009. Eurocode 5 - Design of timber structures - Part 1-1: General-common rules and rules for buildings. European Committee for Standardization (CEN), Brussels, Belgium.

[3] Branco J, Araújo JP (2012). Structural behaviour of log timber walls under lateral in-plane loads. Engineering Structures, 40: 371-382.

[4] Bedon C, Fragiacomo M, Amadio C, Sadoch C (2014). Experimental study and numerical investigation of Blockhaus shear walls subjected to in-plane seismic loads. Journal of Structural Engineering, published online, DOI: 10.1061/(ASCE)ST.1943-541X.0001065.

[5] Hirai T, Kimura T, Yanaga K, Sasaki Y, Koizumi A (2004). Lateral resistance of log constructions. Proc. of WCTE 2004 (CD-ROM), Vol. 1.

[6] Heimeshoff B, Kneidl R (1992). Zur Abtragung vertikaler Lasten in Blockwänden – Experimentelle Untersuchungen [Log-walls under vertical loads – Experimental investigations]. Holz als Roh-und Werkstoff 50:173-180.

[7] Heimeshoff B, Kneidl R (1992). Bemessungsverfahren zur Abtragung vertikaler Lasten in Blockwänden [Design method for log-walls under vertical loads]. Holz als Roh-und Werkstoff 50: 441-448.

[8] DIN1052 Teil 1: Holzbauwerke; Berechnung and Ausführung, 1988.

[9] Eilering S, Beißner E (2011). Zur Stabilität von BSH-Kreisbogenbindern [On the stability of circular curved beams of glued-laminated timber]. Bauingenieur, 86(2): 76-83.

[10] Bouras F, Chaplain M, Nafa Z, Breysse D, Tran H (2012). Experimental behavior of wood columns under extreme loading: cyclic buckling. Proceedings of the World Conference on Timber Engineering WCTE 2012, Volume 5, pp.545-550.

[11] Hofmann R, Kuhlmann U (2010). Influence of creep on the lateral torsional buckling of glued laminated timber girders. Proceedings of 11th World Conference on Timber Engineering WCTE 2010, Volume 1, pp.335-342.

[12] Bedon, C., Fragiacomo, M., Amadio, C., Battisti, A. 2014. Buckling of Blockhaus walls under in-plane vertical loads. Proc. WCTE2014, 10-14 August 2014, Quebec City, Canada.

[13] Bedon C, Fragiacomo M (2015). Numerical and analytical assessment of the buckling behaviour of Blockhaus log-walls under in-plane compression. Engineering Structures, 82: 134-150.

[14] Timoshenko SP, Gere JM (1961). Theory of Elastic Stability, McGraw-Hill, International Book Company.

[15] Wolmir AS (1962). Biegsame Platten und Schalen, VEB Verlag für Bauwesen. Berlin.

[16] EN 338. Structural timber-strength classes. European Committee for Standardization (CEN), Brussels, Belgium; 2009.

[17] EN 301. Adhesives, phenolic and aminoplastic for load-bearing timber structures – Classification and performance requirements. European Committee for Standardization (CEN), Brussels, Belgium; 2006.

[18] UNI EN 408. Timber structures – Structural timber and glued laminated timber – Determination of some physical and mechanical properties [Italian translation]. European Committee for Standardization (CEN), Brussels, Belgium; 2004.

[19] UNI EN 14358. Timber structures – Calculation of characteristic 5-percentile values and acceptance criteria for a sample [Italian translation]. European Committee for Standardization (CEN), Brussels, Belgium; 2007.

[20] Bodig J, Jayne BA (1982). Mechanics of wood and wood composites. Van Nostrand Reinhold, New York.

Figure 1

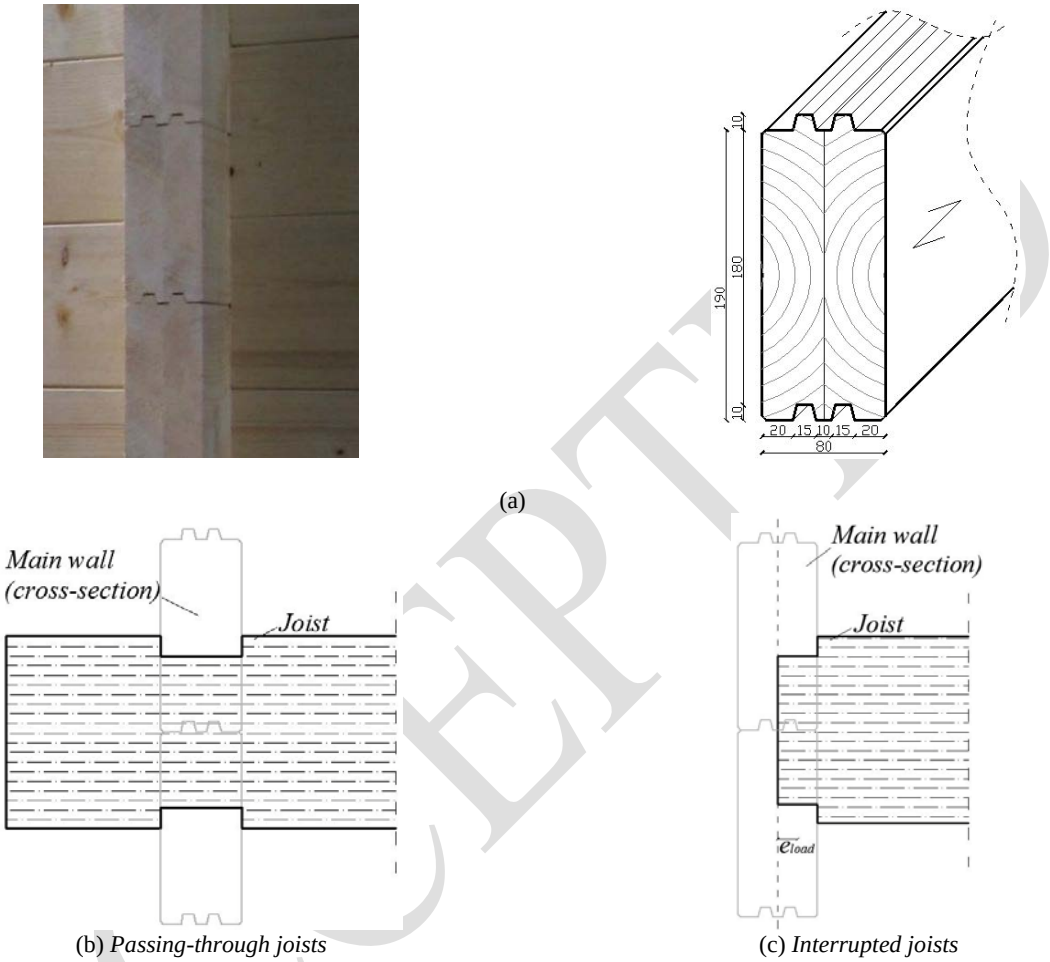

(a)

(b) *Passing-through joists*

(c) *Interrupted joists*

Fig.1. Example of (a) 'Tirol' cross-section (nominal dimensions in mm) and (b), (c) vertical cross-sections of a log-wall to inter-storey floor connection [1].

Figure 2

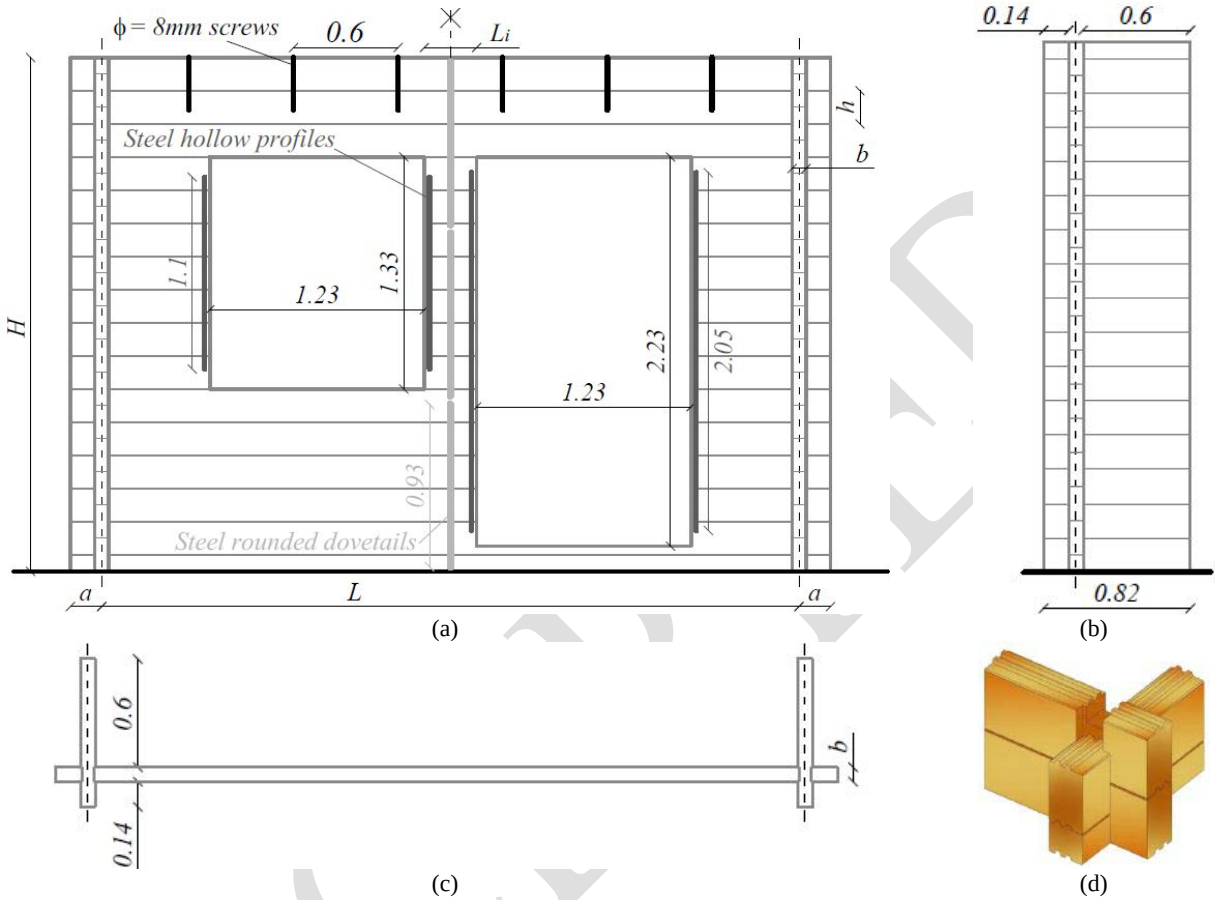

Fig.2. Typical layout of full-scale *Blockhaus* specimens W01-W04 [4].(a) elevation; (b) lateral view; (c) top view; (d) 'Standard' corner joint. Nominal dimensions in m.

Figure 3

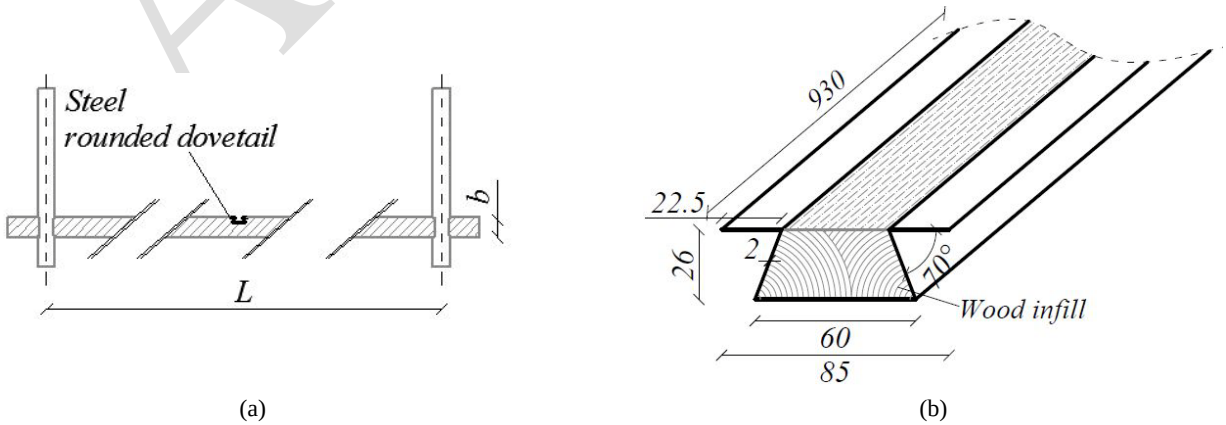

Fig.3. Specimen W02 with 'Standard' corner joints and mid-span steel rounded dovetail profiles. (a) top view of specimen; (b) cross-section of steel profiles (nominal dimensions in mm).

Figure 4

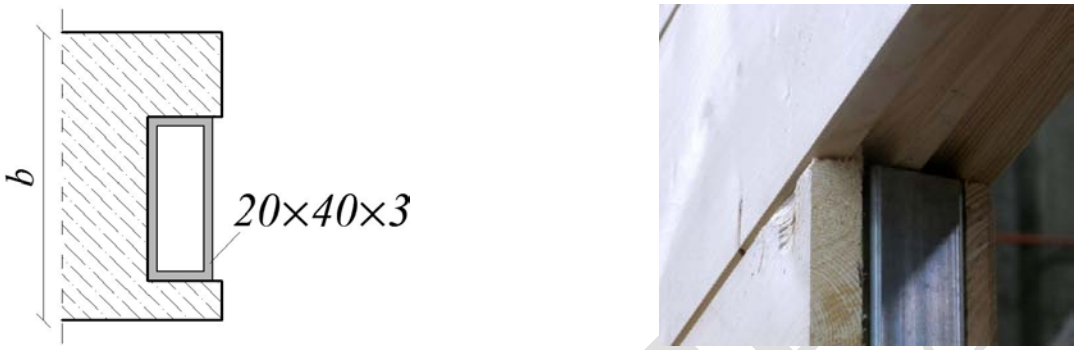

(a) (b)

Fig.4. Steel hollow profiles introduced along the vertical edges of openings (specimens W03 and W04). (a) Nominal cross-section, dimensions in mm; (b) detail near the top corners of the door opening.

Figure 5

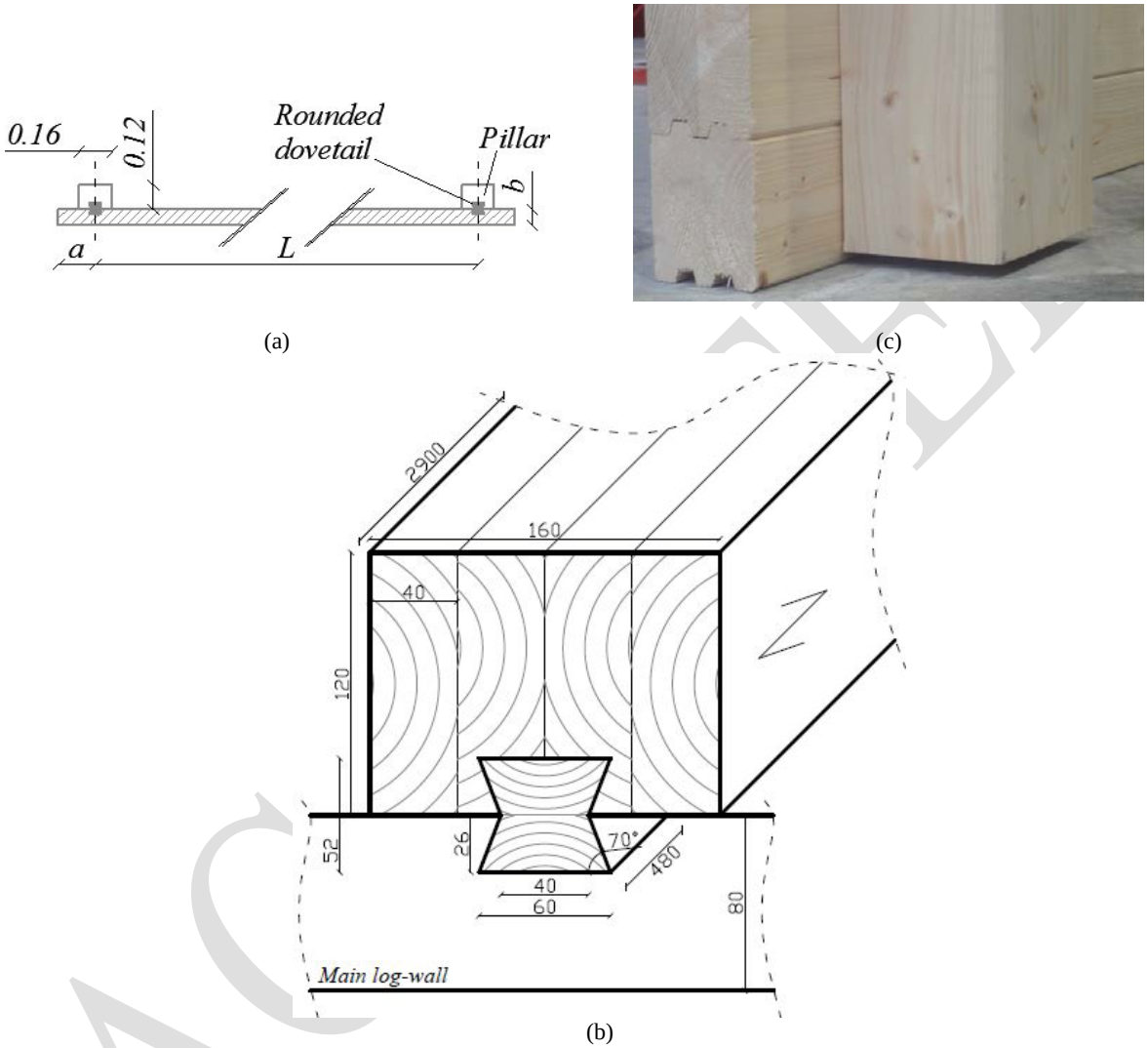

Fig.5. Specimen W05 with timber pillars. (a) Top view of specimen W05 (nominal dimensions in m); (b) detail of the log-wall-to-pillar connection, with nominal dimensions in mm; (c) detail of the base support for pillars.

Figure 6

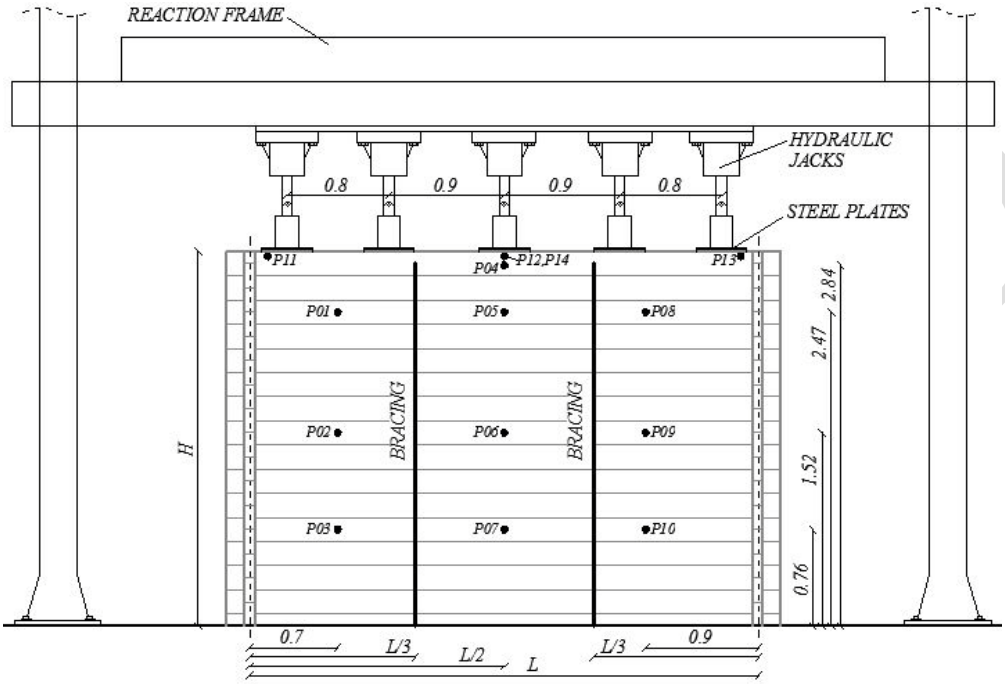

(a)

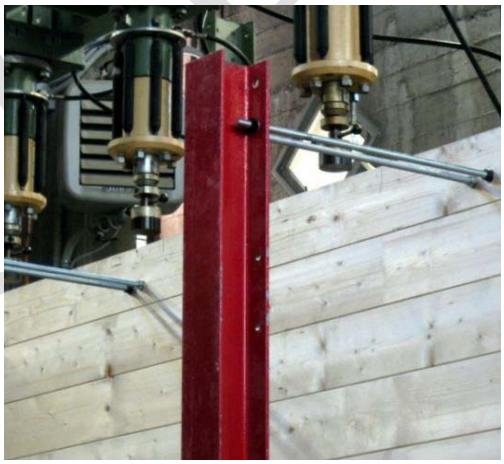

(b)

Fig.6. Experimental setup for the full-scale buckling experiments. (a) Elevation with position of instrumentation (nominal dimensions in m). P01-P10 instruments measuring the horizontal displacements and P11-P14 instruments measuring the vertical displacements; (b) detail of connection between the top timber log of specimens and the metal bracings.

Figure 7

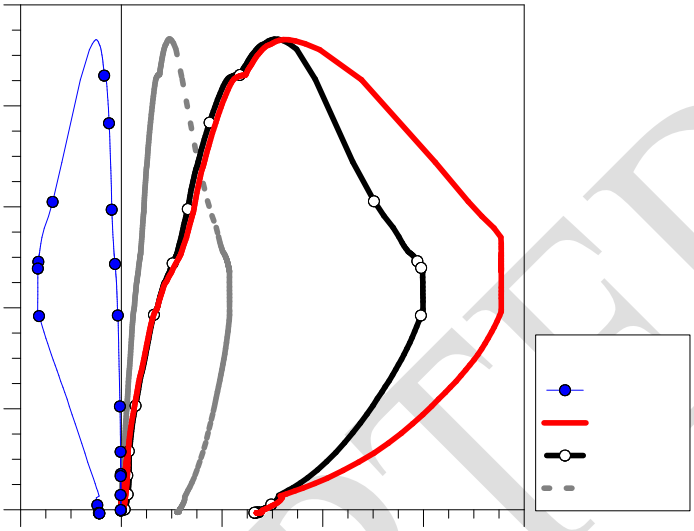

Fig.7. Test results for specimen W01. Load N – horizontal displacement u to height H ratio at control points P04-P07.

Figure 8

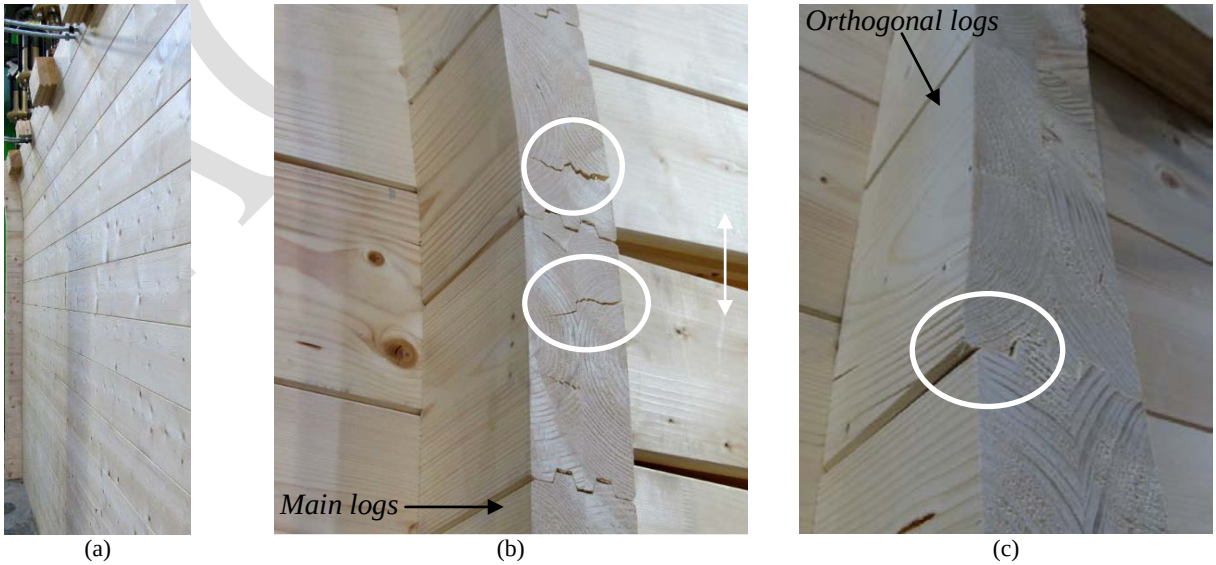

(a) (b) (c)

Fig.8. Failure mechanisms of specimen W01. (a) Overall deformed shape; (b) local damage at the end of main top logs and (c) beginning of crushing at the end of few orthogonal logs.

Figure 9

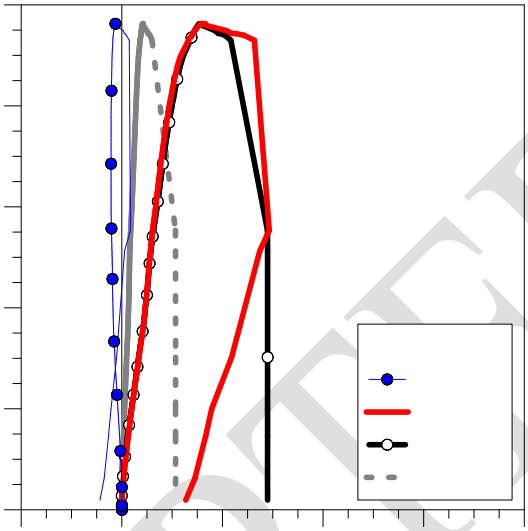

Fig.9. Test results for specimen W02. Load *N* – horizontal displacement *u* to height *H* ratio at control points P04-P07.

Figure 10

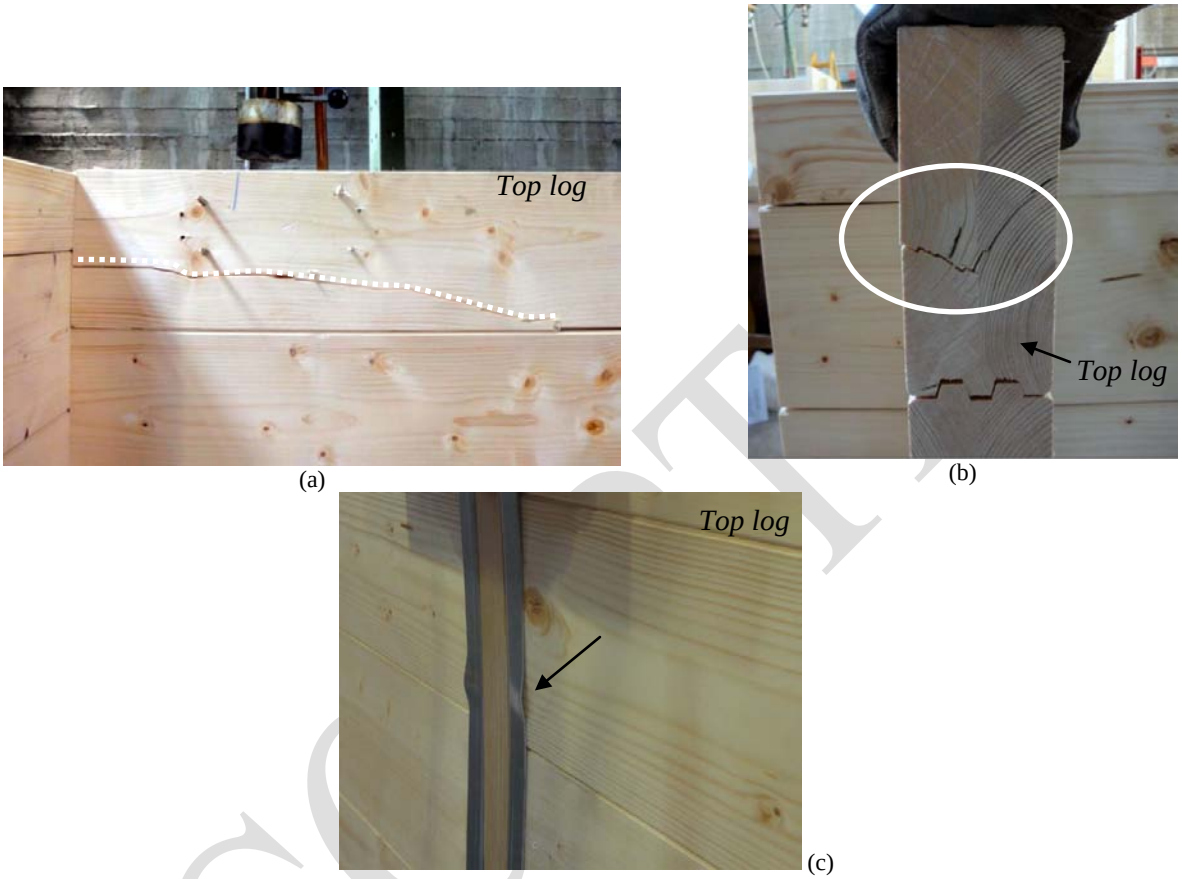

(a) (b) (c)

Fig.10. Failure mechanisms of specimen W02. (a), (b) Detail of flexural damage mechanism in the timber top log, front view and lateral view respectively. (c) Local damage of the upper metal stiffener.

Figure 11

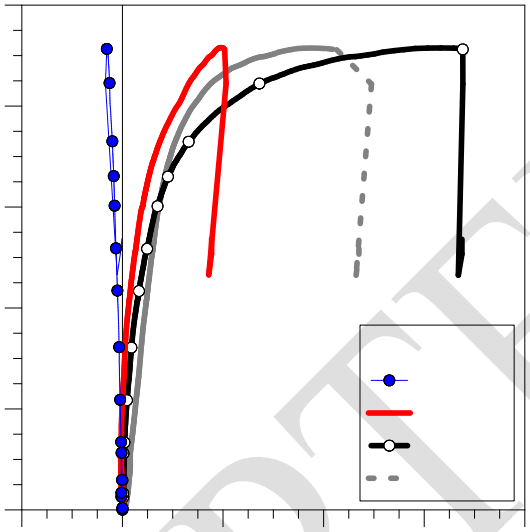

Fig.11. Test results for specimen W03. Load *N* – horizontal displacement *u* to height *H* ratio at control points P04-P07.

Figure 12

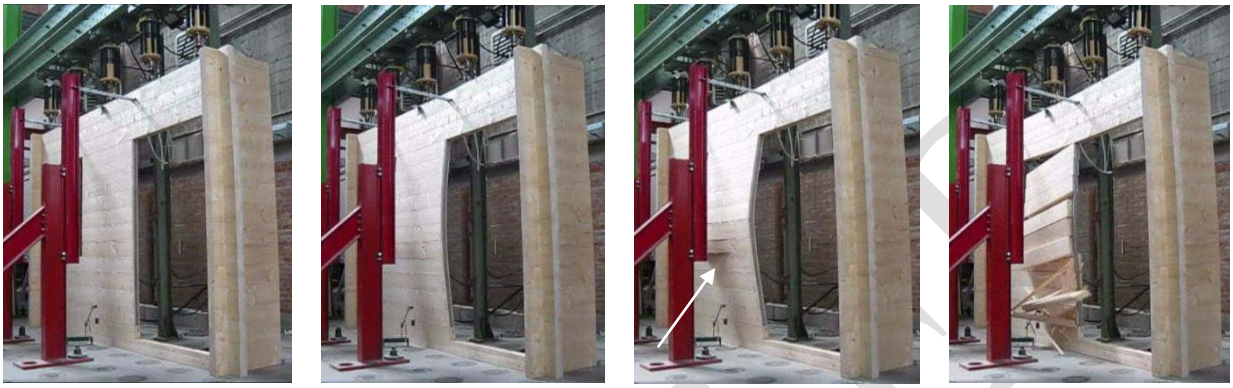

(a)

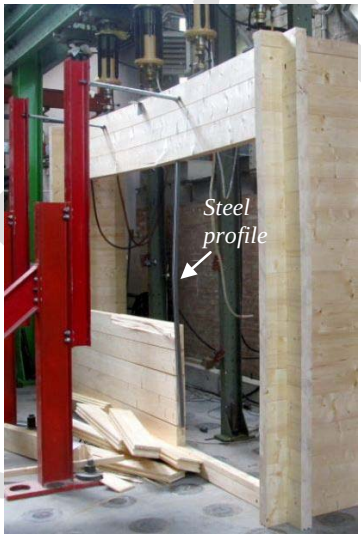

(b)

Fig.12. Collapse mechanism of specimen W03. (a) Sequence of progressive cracking; (b) configuration at the end of the test; (c) detail of damage mechanism in the timber log at the base of the window opening.

Figure 13

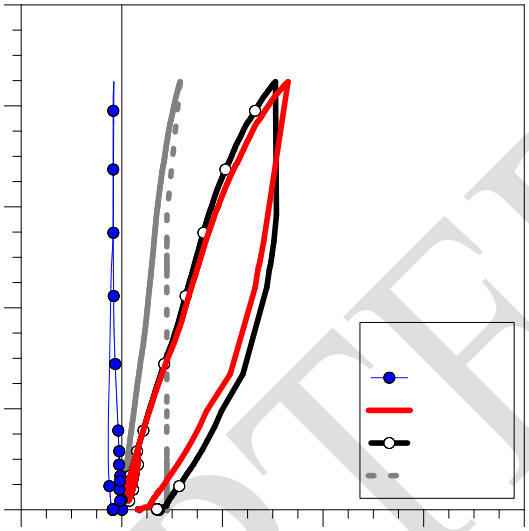

Fig.13. Test results for specimen W04. Load N – horizontal displacement u to height H ratio at control points P04-P07.

Figure 14

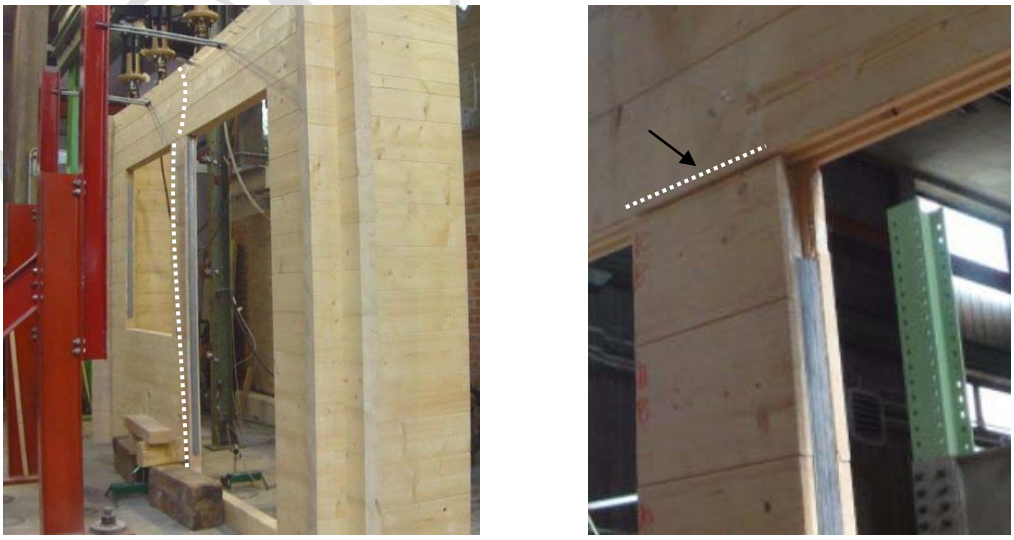

(a) (b)

Fig.14. Deformed configuration at N_{max} of specimen W04. (a) Overview and (b) detail at the connection between the central portion of wall and the top logs.

Figure 15

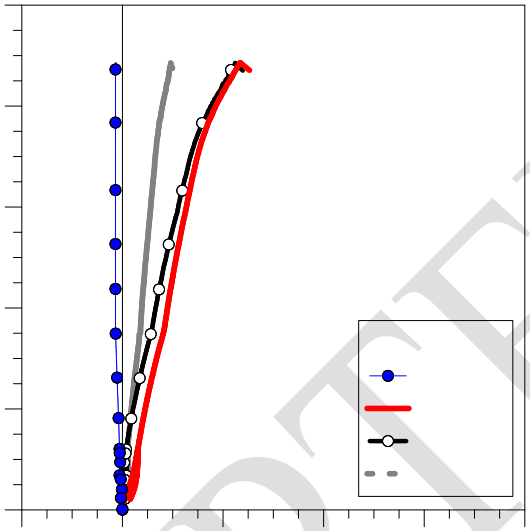

Fig.15. Test results for specimen W05. Load N – horizontal displacement u to height H ratio at control points P04-P07.

Figure 16

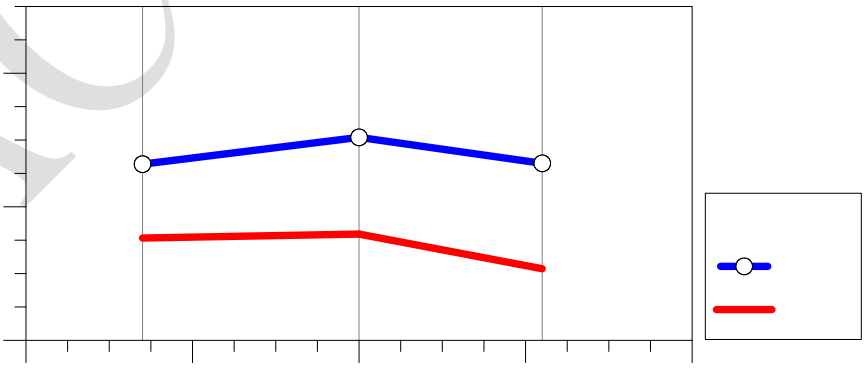

Fig.16. Test results for specimens W01 and W05. Horizontal displacement u to height H ratio at control points P02, P06 and P09. Failure configuration (N/N_{max}= 1).

Figure 17

Fig.17. Collapse mechanism of specimen W05. Sequence of progressive cracking. In the circle, the area of crack initiation.

Figure 18

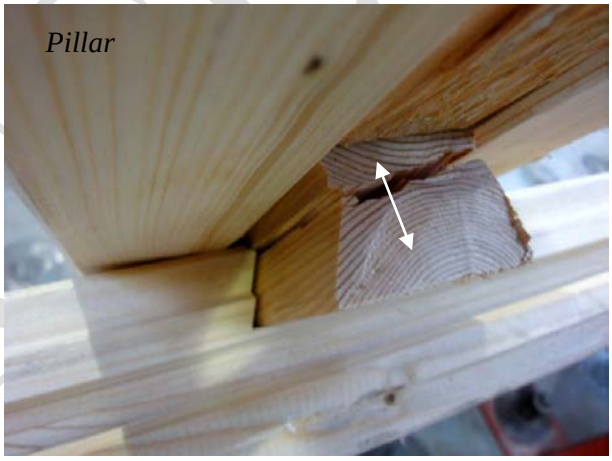

Fig.18. Collapse mechanism of specimen W05. Details of failure mechanism in the rounded dovetails.

Figure 19

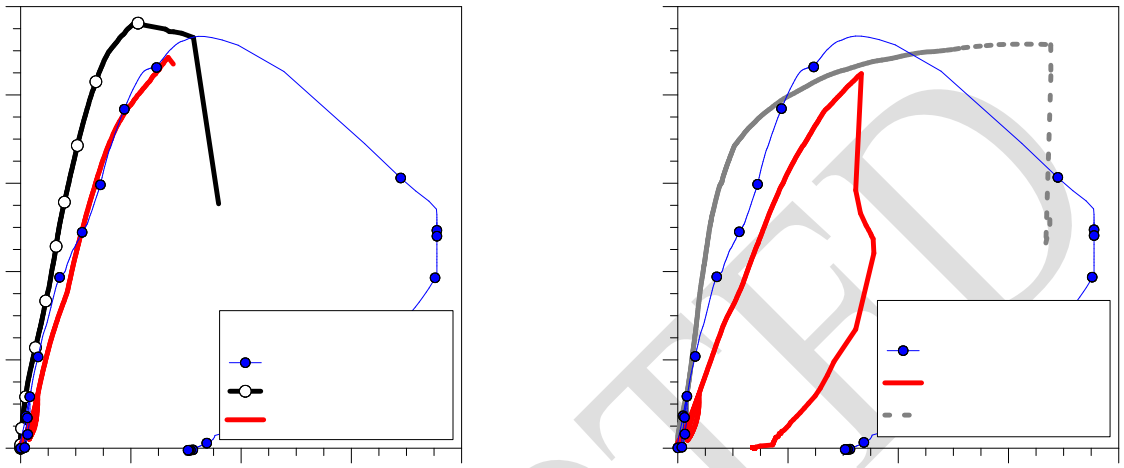

(a) (b)

Fig.19. Test results for specimens (a) W01, W02, W05 without openings; (b) W03, W04 with openings.
Load *N* vs. maximum horizontal displacement *u* to height *H* ratio (max. envelope at control points P01-P10).

Figure 20

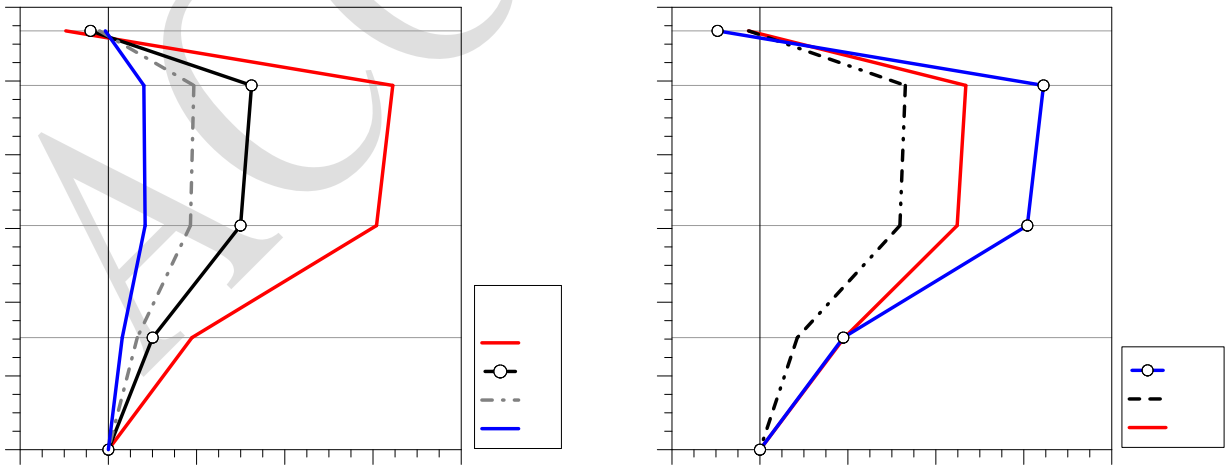

(a) (b)

Fig.20. Test results for specimens without openings. Out-of-plane deformations for (a) specimen W01, at different loading ratios N/N_{max}, along the central vertical portion of the wall (control points P04-P07);
(b) comparative deformed shapes at failure (N/N_{max}= 1) for specimens W01, W02, W05 (control points P04-P07).

Figure 21

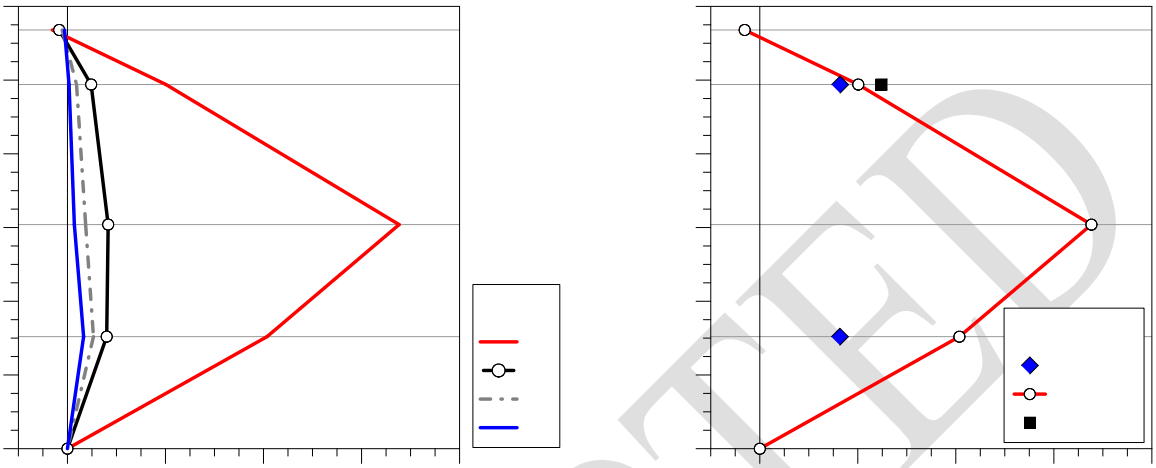

(a) (b)

Fig.21. Test results of specimen W03. Out-of-plane deformations (a) at different loading ratios N/N_{max}, along the central portion of wall (control points P04-P07) and (b) at failure (N/N_{max}= 1) (control points P01-P08).

Figure 22

(a) (b)

(c)

Fig.22. Experiments on small *Blockhaus* specimens. Failure configurations for (a) 'Tirol' log samples and (b) rounded dovetail samples. (c) Bending experiments for the estimation of the longitudinal shear modulus *G*.

Figure 23

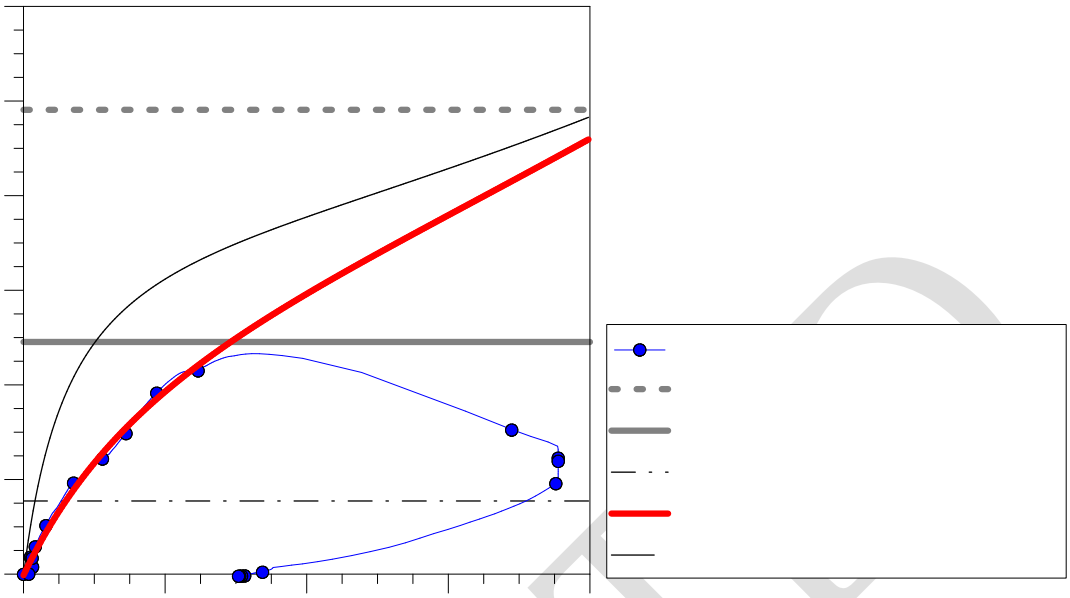

Fig.23. Experimental and analytical (Eqs.(4)-(5), and [7]) comparisons at control point P06 for specimen W01 (e_{load}= b/2= 40mm). Load N versus horizontal displacement u to height H ratio.

Figure 24

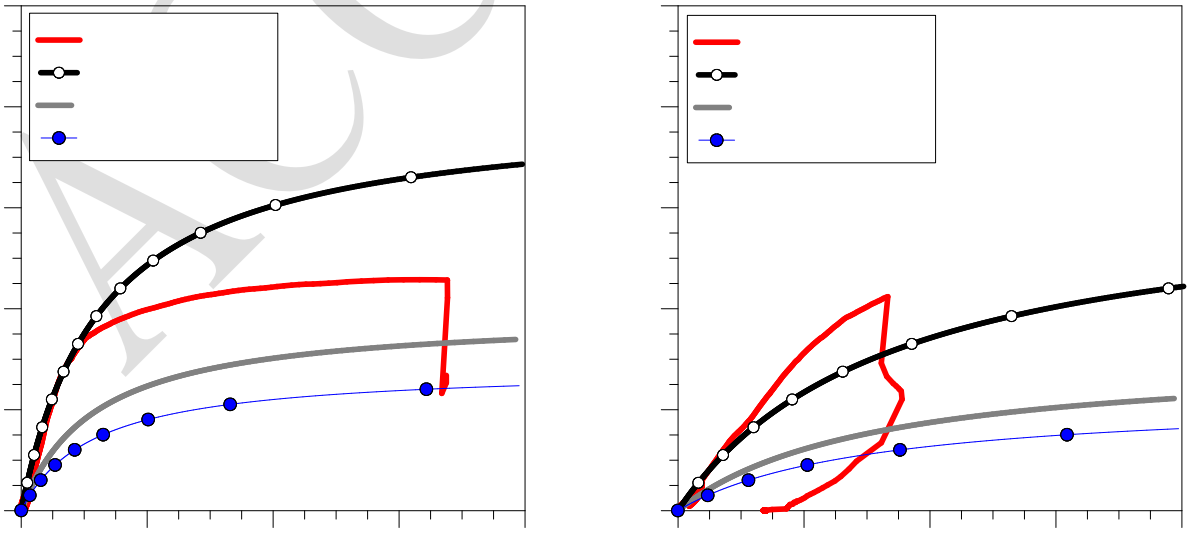

(a) (b)

Fig.24. Experimental and analytical (Eqs.(8), (9) and [7]) comparisons at control point P06 for specimens (a) W03 (e_{load}= 15mm) and (b) W04 (e_{load}= 40mm). Load N versus horizontal displacement u to height H ratio.

Table 1

Table 1. Geometrical properties of full-scale *Blockhaus* specimens. L= 4m, H= 2.945m and b= 0.08m ('Tirol' logs).
* metal rounded dovetail stiffeners.

Specimen	Lateral restraints			Openings					Details
	Type	Joint	a [m]	Type	L_i [m]	L_d, L_w [m]	H_d [m]	H_w [m]	
W01	Orthogonal 'Tirol' log-walls	'Standard' (Fig.2d)	0.18	-	-	-	-	-	-
W02 *									Fig.3
W03				Door + window	1.18	1.23	2.23	1.33	Fig.4
W04					0.30				Fig.4
W05	Pillars	Rounded dovetail		-	-	-	-	-	Fig.5

Table 2

Table 2. Buckling test results obtained for *Blockhaus* full-scale specimens W01-W05.
R_i = test result of the i-test divided by the test result of the 'reference' W01 specimen.

Test		Test results					
Specimen	Load eccentricity e_{load} [mm]	Max. Load N_{max} [kN]	R_N	$u(N_{max})$ / H	$R_{u/H}$	Initial stiffness K [kN/m]	R_K
W01	40	233.2	*1.00*	0.0161	*1.00*	7917	*1.00*
W02	40	240.7	*1.03*	0.0108	*0.67*	11445	*1.45*
W03	15	228.7	*0.98*	0.0316	*1.96*	13590	*1.72*
W04	40	211.9	*0.91*	0.0167	*1.04*	5476	*0.69*
W05	40	221.3	*0.95*	0.0134	*0.83*	7513	*0.95*

Table 3

Table 3. Test results for type (a) *Blockhaus* specimens ('Tirol' logs).

Specimen	Failure stress $\sigma_{u,\perp}$ [N/mm^2]	Mean MOE $E_{\perp}$ [N/mm^2]
T1	3.52	240.8
T2	3.60	154.5
T3	3.59	174.9
T4	3.25	202.4
T5	3.24	208.9
T6	3.09	166.1
Average	*3.39*	*191.25*
CoV [%]	*6.37*	*16.77*
Estimated characteristic 5-percentile value [19]	*2.46*	*107.18*

Table 4

Table 4. Test results for type (b) – pillars – and type (c) – rounded dovetails - *Blockhaus* specimens.

Specimen		Failure stress $\sigma_{u,\parallel}$ [N/mm^2]	Mean MOE $E_{\parallel}$ [N/mm^2]
(b)	P1	33.35	13994
	P2	33.87	11191
	P3	33.55	9485
	Average	*33.59*	*11556*
	CoV [%]	*0.78*	*19.70*
	Estimated characteristic 5-percentile value [19]	*32.78*	*6169*
(c)	R1	52.98	12879
	R2	51.64	13801
	R3	53.07	11672
	Average	*52.56*	*12784*
	CoV [%]	*1.53*	*8.35*
	Estimated characteristic 5-percentile value [19]	*50.08*	*9784*

Table 5

Table 5. Experimental and analytical prediction of the buckling resistance of specimens W01-W05.
(i) Eq.(4); (ii) [7]; (iii) pure compressive resistance;
(I) Eq.(8), with β= 0.699 (clamp-pinned column) and H_{ref}= H_w; (II) Eq.(8), with β= 1 (pinned-pinned) and H_{ref}= H_w;
(III) Eq.(8), with β= 0.699 (clamp-pinned column) and H_{ref}= H_d.

Specimen	Max. Load N_{max}	Predicted critical buckling load N_{cr}			Predicted compressive resistance N_c (iii)
		Calculation method	e_{load}= 0	$e_{load}\neq 0$	
	[kN]		[kN]	[kN]	[kN]
W01	233.2	(i)	490.7	245.3	1084.8
		(ii)	77.3	-	
W02	240.7	(i)	490.7	245.3	1084.8
		(ii)	77.3	-	
W03	228.7	(I)	397.8	323.2	417.6
		(II)	194.4	157.9	
		(III)	141.5	114.9	
		(ii)	69.4	-	
W04	211.9	(I)	315.9	157.9	417.6
		(II)	154.3	77.1	
		(III)	112.3	56.1	
		(ii)	57.6	-	
W05	221.3	(I)	490.7	245.3	1084.8
		(ii)	77.3	-	